Available online at www.sciencedirect.com
SCIENCE DIRECT®
ELSEVIER
Earth and Planetary Science Letters 214 (2003) 633–643
EPSL
www.elsevier.com/locate/epsl

A numerical study of passive transport through fault zones

G.S. O'Brien [a,*], C.J. Bean [a], F. McDermott [b]

[a] *Seismology and Computational Rock Physics Laboratory, Department of Geology, University College Dublin, Belfield, Dublin, Ireland*
[b] *Department of Geology, University College Dublin, Belfield, Dublin, Ireland*

Received 10 March 2003; received in revised form 10 July 2003; accepted 17 July 2003

Abstract

We have numerically simulated contaminant transport through heterogeneous fault zones that consist of three components: a core, a damaged zone and a protolith, each with a different permeability. The interface between each of the components was assigned a fractal topography. This was done to quantify the scaling of a contaminant plume through a fault, as large-scale faults can dominate regional flow. The numerical method used was a modified lattice gas scheme for flow in porous media, coupled to a finite-difference solution to the advection–dispersion equation. The introduction of heterogeneity leads to complex behaviour of a chemical plume in several faults with the same statistical properties. A range of arrival times is observed along with bimodal break-through curves. This behaviour was a common feature in each heterogeneous fault model. The mean and the variance of the plume were calculated for every simulation and indicated that the transport is anomalous. The mean scaled through time from $t^{1.00}$ to $t^{0.54}$ for the different models. Thus, the mean velocity decreased with time in each of the fault models. The minimum and maximum scaling through time of the variance of the plume was from $t^{1.0}$ to $t^{1.87}$ indicating anomalous transport. The simulated break-through curves were analysed using the continuous time random walk method that quantifies the scaling of migrating contaminants using a single parameter β. For $\beta > 2$ the transport is Gaussian and for $\beta < 2$ the transport is anomalous and the variance scales as $t^{(3-\beta)}$ for $1 < \beta < 2$. The average value of β for the different models ranged from 1.65 to 2.00. We have also shown that the scaling of the transport can vary significantly over short distances relative to the size of our models.

Keywords: passive transport; anomalous transport; fault zone; numerical model

1. Introduction

The transport of dissolved chemical species is an important area of research in geological sciences. Results have implications in many fields including waste disposal and the location of nuclear repositories. To accurately model transport through geological media, any model must include heterogeneity, as fracture apertures and fault networks can obey fractal and multifractal statistics [1,2]. Transport through geological media has been shown to exhibit non-Gaussian behaviour as a consequence of heterogeneous flow fields [3,4]. In most models the fracture geometry

* Corresponding author.
E-mail addresses: gareth.obrien@ucd.ie (G.S. O'Brien), chris.bean@ucd.ie (C.J. Bean), frank.mcdermott@ucd.ie (F. McDermott).

0012-821X/03/$ – see front matter © 2003 Elsevier B.V. All rights reserved.
doi:10.1016/S0012-821X(03)00398-4

is represented by planar structures, and the permeability within the fractures and the surrounding rock matrix is homogeneous. In fault networks a small percentage of larger faults can control the flow properties throughout the network. Therefore the transport properties of individual large faults are important in understanding the evolution of regional fluid transport. In contrast with most of the recent research that has concentrated on quantifying contaminant transport through fracture networks, we have focused on the transport of chemical plumes through single large fault structures. Individual fault zones can be represented by a network with an anisotropic distribution of fracture orientations. We have taken a different approach where we consider a faulted zone as a system comprising three distinct units, the core, the damaged zone and the protolith. This should enable us to: (i) test whether fault zones can be treated as planar structures in modelling transport through fault networks and (ii) quantify the scaling of the transport through heterogeneous fault zones. In this paper several different fault zone models, based on field measurements, have been generated to examine the transport of an inert chemical plume. We apply a novel method for passive transport in fault zones, whose lengths are of the order of 200 m, with the inclusion of heterogeneous interfaces separating the different fault zone components. The resultant concentration plumes and break-through curves are then analysed to quantify the transport through fault zones. The method used to model the passive transport is outlined in Section 2, while the numerically generated fault zones are discussed in Section 3. Section 4 presents the results of our numerical simulations and Section 5 discusses these results in terms of the scaling of the chemical plume. The first and second moment of the concentration plume were calculated at different time intervals giving the scaling of the mean and the variance. However, in the vast majority of physical cases a complete description of the plume is unavailable and the only information available is the break-through curves. Therefore, the simulated break-through curves are analysed using the continuous time random walk method (CTRW) [3] as another means of examining the scaling of the plume through the fault zone. The conclusions are presented in Section 6.

2. Numerical scheme

We model flow in heterogeneous porous media using a modified Bhatnagar–Gross–Krook (BGK) method. The BGK scheme is a lattice gas method for the solution of the incompressible Navier–Stokes equation [5]. The modified scheme [6,7] replaces the Boolean nature of the void sites in the lattice gas with a porosity value which enables the scheme to model flow in an arbitrarily scaling heterogeneous porosity distribution. The scheme is coupled with a finite-difference (FD) solution to the advection–dispersion equation:

$$\frac{\partial C}{\partial t} + v_i \frac{\partial C}{\partial x_i} - \frac{\partial}{\partial x_i}\left(D_{ij} \frac{\partial C}{\partial x_j} \right) = 0 \tag{1}$$

where C is the concentration of the species, v_i is the velocity in the x_i direction and D_{ij} are components of the dispersion tensor. The dispersion tensor components D_{ij} were calculated from the expressions:

$$\mathbf{D} = \frac{a_{\mathrm{L}} \mathbf{V} \otimes \mathbf{V} + a_{\mathrm{T}}^{|} \mathbf{V} \otimes^{|} \mathbf{V}}{\| \mathbf{V} \|} \tag{2}$$

from [8] where a_{L} and a_{T} are the longitudinal and transverse dispersivities, and $\mathbf{V}$ is the velocity, $^{|}\mathbf{V}$ is the direct orthogonal to $\mathbf{V}$ and $\otimes$ is the tensor product. The dispersivities are a measure of the amount of spreading of a group of tracer particles. The dispersion tensor accounts for this spreading which is caused by microscopic fluctuations in the velocity of a fluid and the presence of a pore system through which the flow takes place. The flow field in heterogeneous media is computed using the modified BGK scheme and is then used as an input to the FD solution. The scheme was tested extensively against analytical solutions for passive transport through homogeneous porous media and against experimental work on transport through heterogeneous porous media using flow cells [9]. This method was chosen as it allows the flow field in an arbitrary scale model to be calculated. Therefore the scheme retains the advantage that the inclusion of a hetero-

geneous porosity field into the model is relatively straightforward without the scale restriction of the BGK method. The scheme is ideally suited to parallel computing and was implemented on a Beowulf cluster.

3. Fault zone model

A fault zone can consist of three main components, the core, the damaged zone and the protolith [10]. Each component can have its own distinct permeability structure (Fig. 1). The core may act as a conduit for flow during deformation, but it may act as a barrier following deformation. The damaged zone consists of fault-related structures including small faults, fractures, veins and folds. The protolith is the undeformed country rock surrounding the fault whose permeability is similar to the host rock. The parameters used in the fault zone models were taken from [10] and [11]. The ratio of the damaged zone width to the damaged zone and core width (denoted by F_m) was measured for several faults by [10] and was found on average to be 0.7. The porosities of the core, the damaged zone and the protolith were set to 5%, 15% and 0.1% respectively. The horizontal permeability of the damaged zone was set to be approximately 50 mD, while the core and protolith have a horizontal permeability of 10 mD and 0.1 mD respectively. The fault zone was assigned a fractal profile with the damaged zone profile given a Hurst exponent of 0.8 with a maximum amplitude of 7.5 m. The core scales with the damaged zone and the ratio of core to damaged zone was varied from 0.6 to 1.0. All of the parameters used in the simulated fault zone are comparable to measured field values from several different faults [10]. Several different realisations of each fault zone model were simulated and the model parameters are listed in Table 1 and are shown in Fig. 1. The tracer was injected as a point source in the centre of the core at the left hand side of each model.

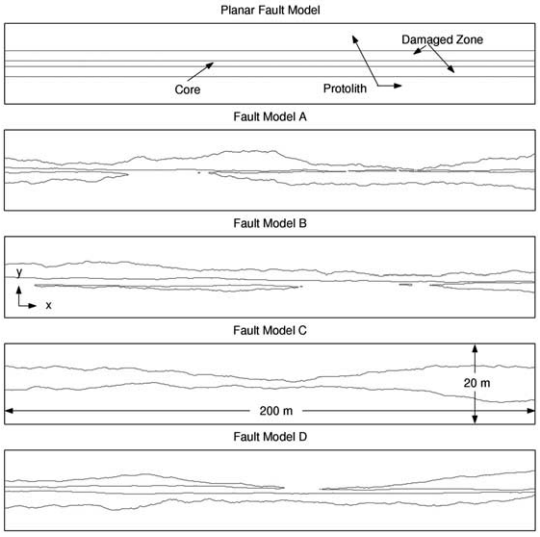

Fig. 1. Fault zone models used in the numerical simulations. The fault zone consists of three main components, the core, the damaged zone and the protolith, each component having its own distinct permeability structure. The parameters used to generate the models are listed in Table 1.

4. Results

In the simulations, a passive tracer was injected as a point source in the centre of the inlet (left-hand side of the fault zone) of each of the different realisations of the fault zone models. Each end of the fault was kept at a constant pressure with the pressure gradient chosen to give a maximum particle flow rate of 1 m/h in a homogeneous permeability of 50 mD. The pressure gradient is glob-

Table 1
The parameters used to generate the fault zone models in the numerical simulations

	Model A	Model B	Model C	Model D	Planar fault model
Hurst exponent	0.83	0.83	0.83	0.83	n/a
Protolith permeability (mD)	0.1	0.1	0.1	4	0.1
F_m	0.70	0.60	1.00	0.70	0.70

The permeability in the fault core was set to 10 mD while the damaged zone permeability was set to 50 mD in all the models. The ratio of the damaged zone width to the damaged zone plus core width is denoted by F_m.

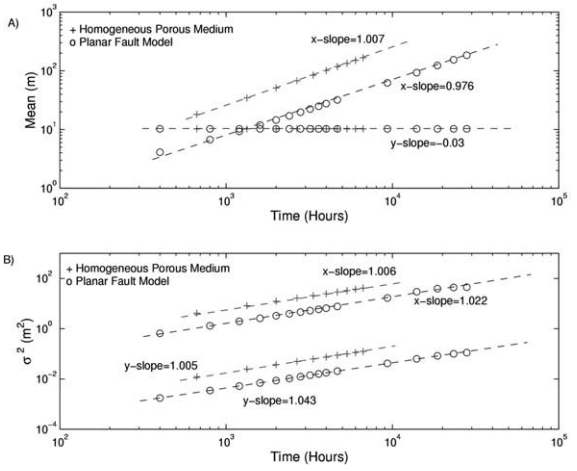

Fig. 2. The log-log plot of the mean (upper panel) and the variance (lower panel) against time for a homogeneous and planar fault model is shown in this figure. A straight line was fitted to the data points using a least squares regression and the slopes show that the scheme replicates Gaussian transport in the homogeneous and planar fault cases. The y-variance in the lower panel has been divided by 100 to improve the clarity of the figure.

al and oriented in the x-direction. This value is arbitrary, as the flow rates in geological systems vary over several orders of magnitude. While the dispersivities may vary spatially and differ in the distinct fault structures, the longitudinal and transverse dispersion coefficients were set to 0.01 m^2/s and 0.001 m^2/s respectively throughout the model. This was done to enable us to examine the effect of heterogeneous interfaces between each of the fault structures. A sensitivity analysis was preformed by changing the dispersion coefficients and hydraulic gradient. The results from these simulations were found to be consistent with the results discussed below.

The homogeneous model and the planar fault model, which represent the standard simulation of faults in numerical modelling, were used as a control for our heterogeneous results. The permeability in the homogeneous model was set to 50 mD while the calculated bulk permeability in the flow direction of the planar fault model was 1.95 mD. The bulk permeability in the flow direction was calculated from Darcy's law using the average flow rate in the direction of flow. This value is an average over the whole fault, so it includes the low-permeability protolith (0.1 mD), the fault core (1 mD) and the high-permeability damaged zone (50 mD). The mean of the concentration plume, calculated using Eqs. 3 and 4, is used to determine the movement of the plume centre.

$$m_x = \frac{\int_{-\infty}^{+\infty}\int_{-\infty}^{+\infty} C(x,y)x\,\mathrm{d}x\mathrm{d}y}{\int_{-\infty}^{+\infty}\int_{-\infty}^{+\infty} C(x,y)\mathrm{d}x\mathrm{d}y} \tag{3}$$

$$m_y = \frac{\int_{-\infty}^{+\infty}\int_{-\infty}^{+\infty} C(x,y)y\,\mathrm{d}x\mathrm{d}y}{\int_{-\infty}^{+\infty}\int_{-\infty}^{+\infty} C(x,y)\mathrm{d}x\mathrm{d}y} \tag{4}$$

The time dependence of the variance (σ) can be found from the concentration plume using Eq. 5 for the x-variance (σ_x) and Eq. 6 for the y-variance (σ_y).

$$\sigma_x^2 = \frac{\int_{-\infty}^{+\infty}\int_{-\infty}^{+\infty} C(x,y)(x-m_x)^2\mathrm{d}x\mathrm{d}y}{\int_{-\infty}^{+\infty}\int_{-\infty}^{+\infty} C(x,y)\mathrm{d}x\mathrm{d}y} \tag{5}$$

$$\sigma_y^2 = \frac{\int_{-\infty}^{+\infty}\int_{-\infty}^{+\infty} C(x,y)(y-m_y)^2\mathrm{d}x\mathrm{d}y}{\int_{-\infty}^{+\infty}\int_{-\infty}^{+\infty} C(x,y)\mathrm{d}x\mathrm{d}y} \tag{6}$$

Using the above equations both the first and second moment of the concentration plume were calculated at different time intervals, giving the scaling of the mean and the variance. In both the homogeneous case and the planar fault case, the x-mean travels as $v = x \cdot t^1$, while there is no variation in the y-position of the concentration plume (Fig. 2A). The x-variance scales as $t^{1.0}$ in the homogeneous case and as $t^{1.02}$ in the planar fault model, while the y-variance scales as $t^{1.0}$ and $t^{1.04}$ in the homogeneous and planar models. In both cases the simulations agree with the expected behaviour of Gaussian transport in homogeneous media and for transport through the planar fault model with the plume centre moving in a straight line at the velocity of the flow.

The introduction of heterogeneity into the fault model leads to a variable velocity field as the fault

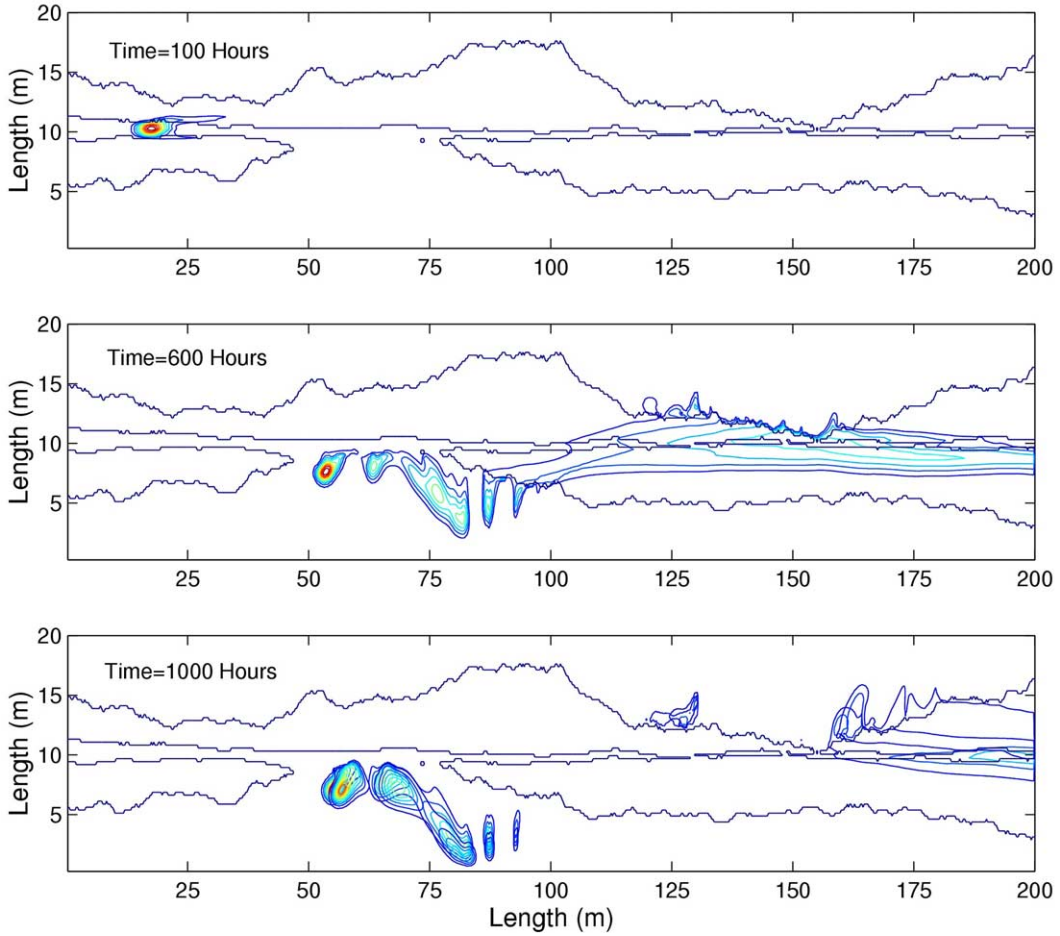

Fig. 3. A contoured plot of the concentration for one of the realisations of model A is shown for different time periods. The *y*-length scale has been exaggerated and the concentration contours have been normalised, maximum is red.

zone broadens and narrows, decreasing and increasing the flow rates. A contoured plot of the concentration for one of the realisations of model A is shown, for different time periods, in Fig. 3. The evolution of the concentration plume becomes complex as it is restricted by the protolith and by the core. The roughness at the boundary between the protolith and damaged zone causes some of the tracer to be trapped. This trapped concentration can slowly escape back into the damaged zone or remain permanently isolated. The storage of material in the protolith is a common problem in pump and treat techniques for contaminant remediation. The break-through curves at three different *x*-locations (30 m, 110 m and 190 m) averaged along the *y*-direction, for five different realisations of model A are shown in log-linear plot in Fig. 4. The log-linear plot was used to highlight the amplitudes of the concentration. The figure clearly shows that the introduction of heterogeneity into the model leads to complex behaviour of the concentration plume. There is a clear variation in the concentration amplitudes as well as in the break-through profiles. The latter point is more clearly illustrated in Fig. 5 where we have plotted the normalised cumulative sum of the break-through concentrations at six different locations through the five realisations of fault zone model A. The figure shows different arrival times and bimodal break-through

curves. From Figs. 4 and 5 it is clear that the behaviour is complex and can vary dramatically over a 200 m length for faults with the same statistical properties. Fig. 6 shows the break-through curves where a tracer is injected as a line source throughout the inlet of the fault zone. Again, the behaviour is complex with multiple break-throughs, and it differs dramatically for each of the different realisations of fault model A. The break-through curves for the different models will be analysed in more detail in Section 5. Fig. 7 shows a contoured plot of the concentration plume for the planar fault model and fault models B, C and D. As expected in the planar fault model, the plume behaves in a Gaussian fashion. The behaviour of the plume in models B, C and D is more complex. In model B the ratio of the damaged zone width to the core width was decreased. In this realisation this has the effect of restricting the transport of material through the fault core. In model C the fault core is removed and the plume spreads out throughout the damaged

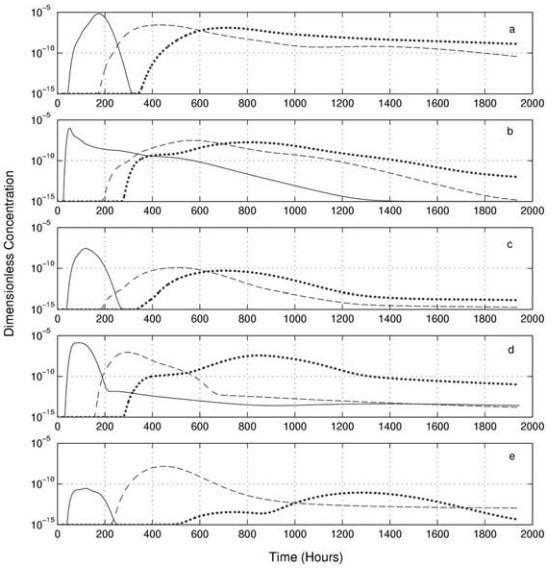

Fig. 4. The break-through curves of five different realisations (a–e) of model A are plotted in log-linear scale. The log-linear scale was used to better highlight the relative amplitudes of the break-through concentration. The solid line represents a breakthrough curve measured at 30 m from the source, the dashed line was measured at 110 m from the source and the dotted line was measured at 190 m from the source. A broad spectrum of different types of behaviour is clearly seen.

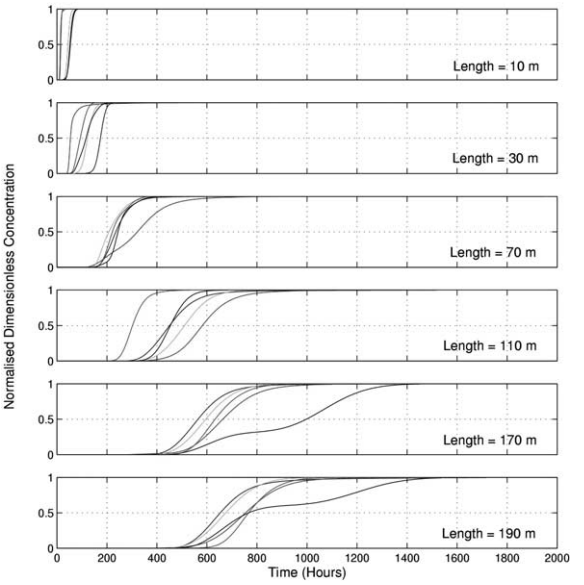

Fig. 5. The figure shows the normalised cumulative sum of the break-through curves from five different realisations of fault model A at different locations. The figure shows different arrival times and bimodal break-through curves implying that the behaviour varies for different faults with the same statistical properties.

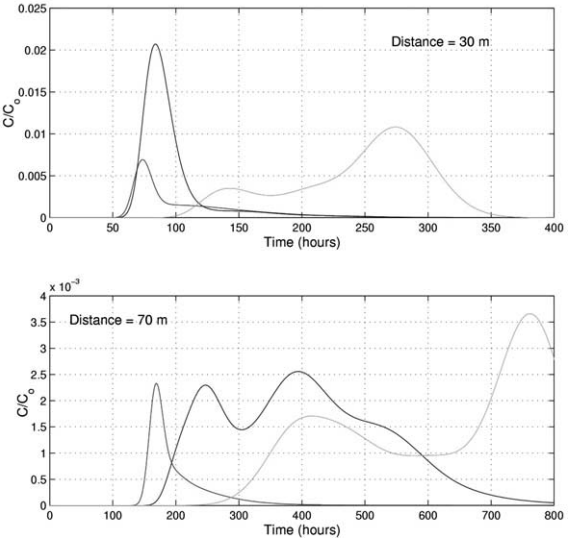

Fig. 6. Break-through curves for different realisations of fault zone model A measured at two distances from a line source input across the entire width of the fault zone (as opposed to the point source shown in Fig. 4). The behaviour is complex and can vary dramatically for different realisations.

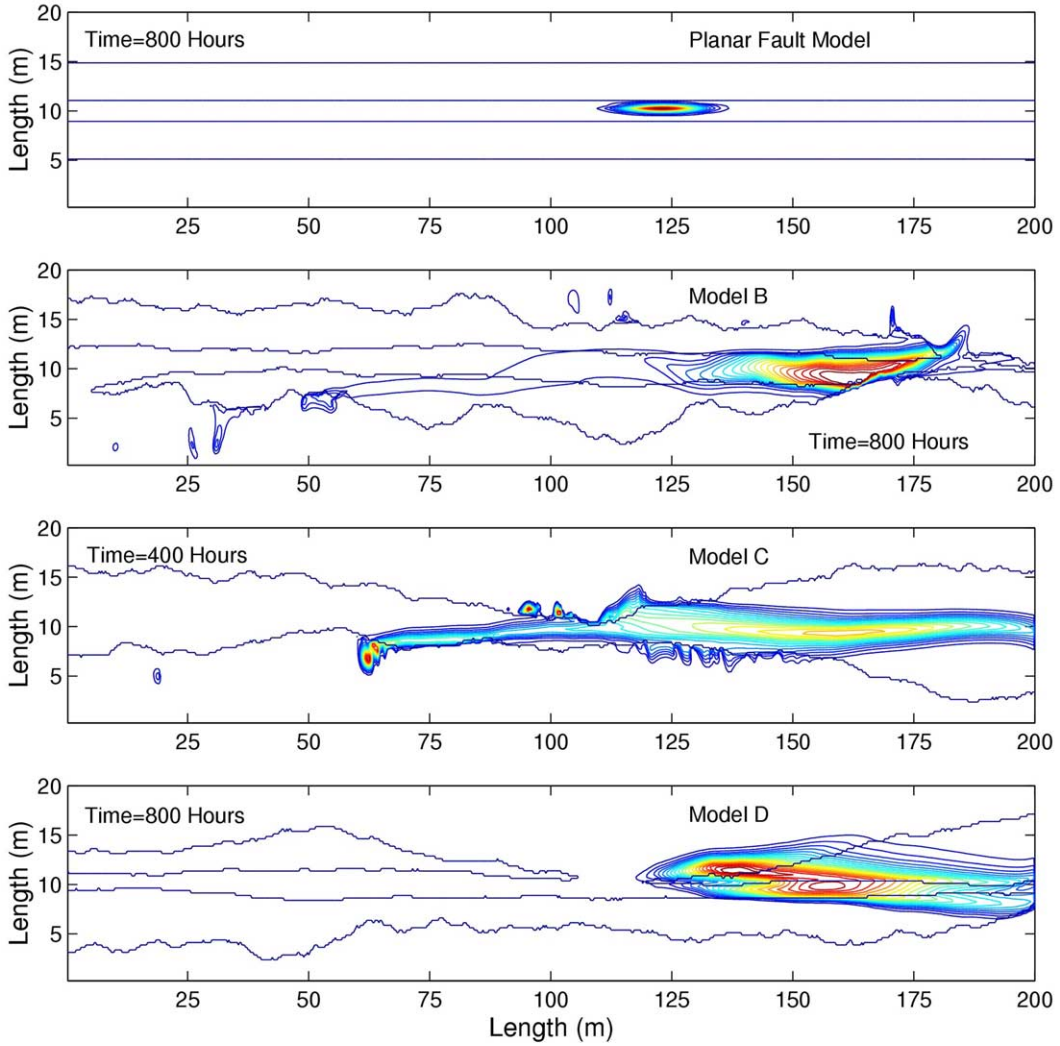

Fig. 7. The concentration plume is shown for a single realisation of each of the fault models. The *y*-length scale has been exaggerated and the concentration contours have been normalised, maximum is red.

zone. As in model A, material can be trapped in the protolith and either stored or released slowly back into the damaged zone. In model D the higher permeability of the protolith allows the tracer to move relatively freely through the fault zone. If the permeability and porosity of the protolith is increased then material that is forced into the protolith can no longer be stored for substantial periods of time. The break-through curves for the fault models are shown in Fig. 8 at three different locations, 30 m, 110 m and 190 m, for three different realisations of each model. As in Fig. 4, a wide variety of behaviour is clearly seen. To examine the effect of the small-scale roughness we ran a simulation where we filtered the fault boundaries of model A with a low-pass filter. As expected, the effect of the small-scale roughness on the transport is minimal. On the scale of the fault zone this result is not surprising as the Hurst exponent of 0.83 provides a relatively smooth interface and therefore the long-wavelength variation plays the dominant role in channelling or trapping the flow. In the planar fault model the break-through curves are regular as expected,

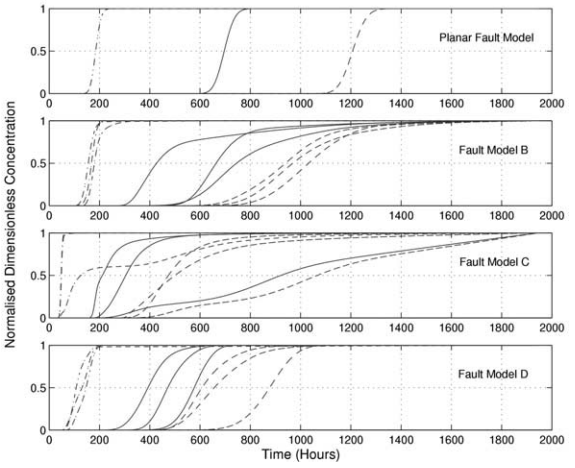

Fig. 8. The figure shows the normalised cumulative sum of the break-through curves from three different realisations of the different fault models. The dashed-dotted line represents a breakthrough curve measured at 30 m from the source, the solid line was measured at 110 m from the source and the dotted line was measured at 190 m from the source. The heterogeneous fault models exhibit bimodal break-throughs and a variation in arrival times.

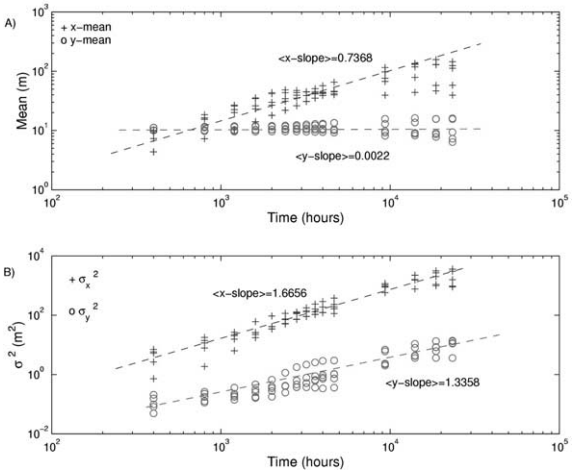

Fig. 9. The log-log plot of the mean (upper panel) and the variance (lower panel) against time for all the realisations of fault model A is shown. A straight line was fitted to the data points using a least squares regression. The centre of plume travels as $t^{0.74}$ in the direction of flow with little variation in the y-direction. The x-variance scales as $t^{0.83}$ and the y-variance scales as $t^{0.67}$. This indicates a super-diffusive process as material is channelled through the fault models.

while a wide variety of arrival times and profiles are seen when heterogeneity is introduced.

5. Discussion of results

In Section 4 we have discussed the results in general terms. In this section we quantify the transport of the concentration plume throughout the fault models. Using Eqs. 3–6 the temporal scaling of the mean and variance of the plume was calculated. Fig. 9 shows the log of the variance against log of time for five different realisations of model A. The plume moves sublinearly and is scattered around the y-direction as expected due to the transport of material through and around the distinct fault structures. The tail-off at later times is due to the finite size of the model as the plume eventually moves beyond the edge of the model. The variance of the plume scales as $t^{1.66}$ and $t^{1.34}$ (the exponents having a standard deviation of 0.285 and 0.352) in the x

Table 2
The average slope of each realisation of the different fault models in a log-log plot of time against the mean and the variance for both the x and y directions

	Model A	Model B	Model C	Model D	Planar fault model	Homogeneous model
n_x	0.737 (0.211)	0.914 (0.047)	0.538 (0.086)	0.890 (0.035)	0.976	1.000
n_y	0.002 (0.089)	0.001 (0.039)	−0.056 (0.090)	0.012 (0.003)	−0.030	0.000
α_x	1.666 (0.285)	1.871 (0.073)	1.678 (0.099)	1.243 (0.254)	1.163	1.006
α_y	1.336 (0.352)	1.199 (0.385)	0.966 (0.254)	0.940 (0.132)	1.043	1.005
$\langle\beta\rangle$	1.769 (0.222)	1.651 (0.260)	1.525 (0.251)	1.952 (0.047)	1.994 (0.010)	2.000
$(3-\langle\beta\rangle)$	1.231	1.349	1.475	1.048	1.006	1.000

The mean scales as t^n and the variance scales as t^α. The figures in parentheses are the standard deviation of the slopes. The average exponent β calculated on simulated break-through curves using CTRW theory throughout the different fault models is also listed in this table. The variance scales as $t^{(3-\beta)}$ for $1<\beta<2$. The values of $(3-\beta)$ also listed in the table agree within the standard deviation of the scaling of the variance from Eqs. 5 and 6.

and y direction respectively. This is a consequence of the plume being channelled through the fault zone. Table 2 shows the scaling of the mean and variance for all the fault models. As discussed earlier, the homogeneous model and planar fault model behave as expected. Model B behaves in a manner similar to model A, with the plume being channelled through the fault zone while model C shows a super-diffusive process in the x-dispersion but the y-variance is close to 1.0. The removal of the core allows the centre of the plume to move in a more undulating manner through the fault. This is reflected in the low value of the slope of the x-mean (0.538) and the high absolute value of the y-mean slope (0.056). In model D, the low contrast in permeability between the damaged zone and protolith allows the plume to disperse relatively freely.

The numerically simulated break-through curves were analysed using the CTRW method. The CTRW method is based on the calculation of probability density functions $\psi(\mathbf{x},t)$ over a distance and direction $\mathbf{x}$ in time t where $\psi(\mathbf{x},t)$ is defined for an ensemble average over many possible realisations of the domain. The plume migration is dominated by the behaviour of $\psi(\mathbf{x},t)$ at 'large times' and the long-term behaviour of $\psi(\mathbf{x},t)$ can be expressed as $\sim t^{-1-\beta}$ with $0<\beta<2$. The variance scales as $t^{(3-\beta)}$ for $1<\beta<2$ with $\beta>2$ implying Gaussian transport and $\beta<2$ implying anomalous transport [3]. The advection–dispersion equation is solved at a 'local scale' producing 'large-scale' break-through curves which are anomalous and quantifiable with the CTRW method. The advection–dispersion equation is insufficient for the analysis of the 'large-scale' break-through curves. A detailed description of the CTRW method can be found in [3,14] and references therein. The method has been used to quantify anomalous transport in fracture networks and highly heterogeneous porous media [12,13].

In any physical experiment or field investigation it is practically impossible to gain a complete description of the concentration plume. The only information in the vast majority of cases is the break-through curves measured at various locations in the site under investigation. Hence it is important to determine how accurate a measure of scaling is actually given by the break-though curves. By fitting the numerically simulated break-though curves to the CTRW theory we can compare the scaling of the variance of the plume from Eqs. 5 and 6 with the scaling obtained from the break-through curves. The numerically simulated curves were fitted to the CTRW theory using the non-linear curve fitting option in GRACE, a detailed description can be found in [15].

Fig. 10 shows the simulated cumulative break-through curves and the CTRW theory curves at three different x-locations in the middle of the fault zone. The scaling exponent β ranges from 1.27 to 1.70 indicating anomalous transport throughout the fault zone model. However, as discussed previously many of the simulated curves show bimodal and complex profiles that cannot be fitted with the CTRW theory. In Fig. 11 we have plotted the variation of β throughout each realisation of the different fault models. In some cases the numerically simulated break-through curves could not be fitted to the CTRW theory for the reasons outlined above. In this case no value of β is shown in the figure. As expected for the planar fault model β is close to 2 throughout the entire fault model. For models A, B and C the value of β close to the source is approximately 2 and it decreases further from the source. This is

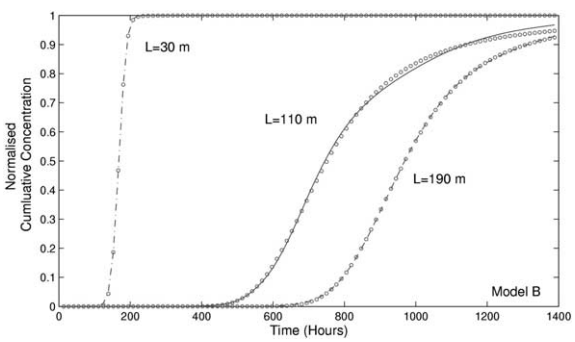

Fig. 10. The numerically simulated break-through curves were fitted against the CTRW theory to quantify the scaling of the transport process. This figure shows three break-through curves from model B. The solid line represents the numerically simulated curves while the circles are the CTRW fit. The scaling exponent β from the CTRW theory is 1.51, 1.27 and 1.70 for $L=30$ m, $L=110$ m and $L=190$ m respectively. The results show that the transport is anomalous.

reasonable, because close to the source, the plume has not encountered enough of the heterogeneous flow field, but as the plume moves further through the fault the influence of the variable flow field grows. From the figures it can been seen that there is a large scatter of β with no clear trend. In model D, β varies very little throughout the fault and remains close to 2. Again, this is consistent with the low contrast in permeability between the damaged zone and protolith. Table 2 shows the average value of β and $(3-\beta)$ throughout the fault zone models. The temporal scaling of the variance using the CTRW method is in good agreement with the temporal scaling using Eqs. 5 and 6 for the concentration plume. While the results appear to match well and show that the transport through the fault is anomalous, caution must be exercised when quantifying the scaling of

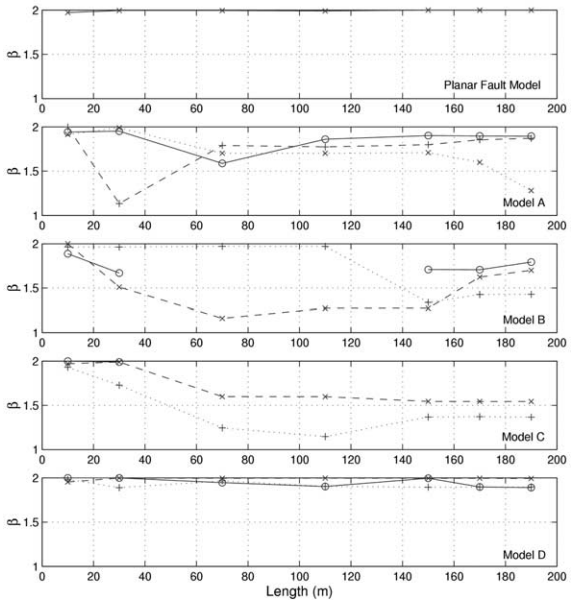

Fig. 11. This figure shows the variation of β throughout each realisation of the different fault models. In some cases β cannot be calculated and hence is not plotted (see text). In the planar fault model β is close to 2 throughout the entire fault model. For models A, B and C the value of β close to the source is approximately 2 and decreases further from the source. As the plume moves further along the fault the variable flow field influences the dispersion and advection of the plume and the transport becomes anomalous. In model D, β varies very little throughout the fault and remains close to 2.

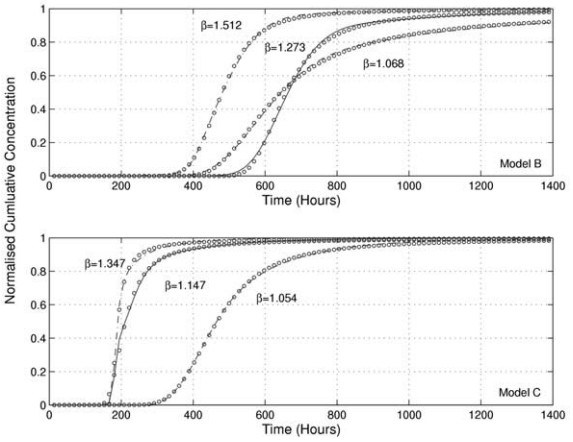

Fig. 12. The break-through curves located less than 5 m from each other are plotted along with the CTRW theory fit for one realisation of models B and C. It can be seen that the transport scaling can differ significantly over very short distances.

the transport process. In field experiments only a few sample locations are typically chosen for various reasons, the cost of drilling wells for example. In each simulation three break-through curves were measured only 5 m apart, and the parameter β was calculated for each of the different locations. Generally β did not vary, but in several simulations the value of β varied between 1.0 and 1.5. In Fig. 12, three break-through curves, located less than 5 m from one another, are plotted along with the CTRW theory fit for one realisation of models B and C. From the figure it can be seen that the transport scaling can differ over very short distances. Model C was included as it only has a damaged zone. This shows that this effect is independent of measuring the curves in the different fault components, as all the curves were sampled in a damaged zone.

6. Conclusions

Modelling of the transport of chemicals through a fault zone is critical in understanding contaminant transport. A homogeneous model and a planar fault zone were used as a control on the combined BGK and finite difference model. In both cases the numerical scheme replicated

the expected behaviour. Heterogeneous fault models constrained from field studies were then used to investigate the effect of passive transport through such media. In the fault zone models, the transport of a passive tracer through the zone was found to be heterogeneous. This is a consequence of the roughness of the boundaries between each component and the interaction between the distinct components within the fault zone. An assortment of different types of behaviour is possible depending on the initial geometry of the fault zone. The zone can be capable of soaking the material and slowly releasing or storing it. The results show that the transport of material through the fault zone is a super-diffusive process, with complex behaviour when heterogeneity is introduced. The size of this non-Gaussian effect depends on the amplitude of the damaged zone profile and the Hurst exponent. By decreasing the damaged zone amplitude relative to the zone width, the non-Gaussian effect disappears, and the zone can be approximated as homogeneous. However, a fault of this nature may not be a realistic model of a true fault zone. Finally, the scaling of the mean and variance of the plume can differ significantly over small distances. As discussed earlier, the fault zone models used are representations of real fault zones in which the dispersivities vary spatially and the permeability within each fault component is heterogeneous. The inclusion of more complex geometry can only increase the complexity of transport through faults. Therefore to accurately model the transport of material through these geological structures a better understanding of fault geometry is necessary. In particular, this has important implications for modelling contaminant transport from waste disposal sites.

Acknowledgements

The authors acknowledge constructive reviews by P. Favreau and three anonymous reviewers that greatly improved the clarity of the manuscript. G.S.O'B. was funded by Cosmogrid Ireland.*[BARD]*

References

[1] W.C. Belfield, Multifractal characteristics of natural apertures, Geophys. Res. Lett. 21 (1994) 2641–2644.
[2] E. Bonnet, O. Bour, N.E. Odling, P. Davy, I. Main, P. Cowie, B. Berkowitz, Scaling of fracture systems in geological media, Rev. Geophys. 39 (2001) 347–383.
[3] B. Berkowitz, H. Scher, Theory of anomalous chemical transport in random fracture networks, Phys. Rev. E 57 (1998) 5858–5869.
[4] G. Kosakowski, B. Berkowitz, H. Scher, Analysis of field observations of tracer transport in a fractured till, J. Cont. Hydrol. 47 (2001) 29–51.
[5] Y. Qian, D. D'Humieres, P. Lallemand, Lattice BGK models for the Navier-Stokes equation, Europhys. Lett. 17 (1992) 479–484.
[6] O. Dardis, J. McCloskey, Lattice Boltzmann with real numbered solid density for the simulations of flow in porous media, Phys. Rev. E 57 (1998) 4834–4837.
[7] O. Dardis, J. McCloskey, Permeability porosity relationships from numerical simulations of fluid flow, Geophys. Res. Lett. 25 (1998) 1471–1474.
[8] J. Bear, Y. Bachmat, Introduction to Modelling of Transport Phenomena, Kluwer Academic, Dordrecht, 1991.
[9] G.S. O'Brien, A Coupled BGK-FD Method for Reactive Fluid Flow in Heterogeneous Porous Media, Ph.D. Thesis, University College, Dublin, 2002.
[10] J.S. Caine, J.P. Evans, C.B. Forster, Fault zone architecture and permeability structure, Geology 24 (1996) 1025–1028.
[11] J.P. Evans, C.B. Forster, J.V. Goddard, Permeability of fault related rocks and implications for hydraulic structure of fault zones, J. Struct. Geol. 19 (1997) 1393–1404.
[12] B. Berkowitz, H. Scher, Anomalous transport in random fracture networks, Phys. Rev. Lett. 79 (1997) 4038–4041.
[13] B. Berkowitz, H. Scher, S. Silliman, Anomalous transport in laboratory-scale, heterogeneous porous media, Water Resour. Res. 36 (2000) 149–158.
[14] G. Margolin, B. Berkowitz, Spatial behaviour of anomalous transport, Phys. Rev. E 65 (2002) 1–11.
[15] B. Berkowitz, H. Scher, The role of probabilistic approaches to transport theory in heterogeneous porous media, Transp. Porous Media 42 (2001) 241–263.